Decoupled Floating Capacitor Voltage Control of a Dual Inverter Drive for an Open-Ended Winding Induction Motor

Chatumal Perera, *Student Member, IEEE*, Gregory J. Kish, *Member, IEEE*, and John Salmon, *Member, IEEE*

***Abstract*—A control scheme is presented for a dual inverter drive with a floating capacitor bridge, with decoupled motor and capacitor dynamics. A stator current reference frame is used that decouples the real and reactive power components of the motor and enables the decoupling of the motor and capacitor dynamics. Apart from the high frequency voltage ripple due to the inverter switching pattern, the capacitor voltage can be kept constant even during large step changes in motor speed reference and load torque. This allows for the use of a significantly smaller floating bridge capacitor whose size depends only on the steady-state high frequency voltage ripple. Additionally, the number of PI regulators used compared to previous works and the dc-link voltage requirements are both reduced.**

***Index Terms*—Dual inverter drive, field oriented control, floating capacitor bridge, open-ended winding induction machine.**

I. Introduction

THE internal combustion engine-based vehicle is gradually being replaced by electric vehicles (EVs) due to their superior performance in terms of efficiency, reliability, cost, and environmental friendliness. Permanent magnet synchronous machines (PMSMs) are ideal for high speed applications such as EVs since they provide high efficiency, torque, and power density [1]. However, the cost and availability of rare-earth metals used to build PMSMs has always been a concern. Thus, researchers have turned their attention toward high speed motor drives based on alternative machines such as induction machines (IMs) which are far more cost effective and more robust to overload conditions [2], [3].

The dual inverter drive (DID) [4] using an open-ended winding induction machine (OEWIM) is a topology suitable for high speed applications such as EVs. This topology has also been proposed for applications such as aerospace [5] and EV fast charging [6] recently. The main advantage of this topology compared to a single inverter is its voltage boost, which extends both the constant torque region [7] and the constant power region [3] of an IM. Apart from this, the multilevel nature of the motor line voltage improves the motor current quality. Compared to the neutral point clamped converter (NPC), the DID has both a lower component count [8] and lower dc-link voltage requirements. It also has more redundant switching states and a higher pulse width modulation (PWM) frequency compared to the NPC, allowing for more flexible PWM schemes [9]. The DID topology has three variants which have different dc supplies. The first configuration [4], [10]–[12] uses two isolated dc supplies which increases its reliability [10]. However, the isolation requirements increase the size, weight, and cost of the drive. The second configuration uses a common dc-link for both inverters [13]–[15]. However, this creates a common mode path for high frequency currents from PWM to flow through the motor which can cause excessive losses. To counter this, PWM schemes that eliminate common mode voltage have been proposed in [13]–[15] at the cost of dc-link utilization and current quality.

The third configuration, the focus of this article, has one inverter supplied by a dc source while the other inverter uses a floating capacitor connected across its dc-link to supply reactive power. This configuration retains the typical DID advantages such as voltage boost and better PWM, while eliminating common mode currents and isolated supply requirements. The complexity of the control for this configuration is higher due to the need for capacitor voltage control. However, the benefits of this configuration easily justify the use of more complex control.

There are two main approaches for controlling this DID configuration in literature. In the first approach [16], [17], and [5], the capacitor voltage is regulated by a PWM scheme by using the redundant states of the drive to charge or discharge the capacitor. Vector control [18] of the motor is also implemented using proportional integral (PI) controllers. This method is based on 4-level space vector (SV) modulation and is designed only for a 2:1 inverter dc-link voltage ratio. Also, the operating power factor of the machine affects the redundant states used for charging and discharging the capacitor. This point is addressed in [5]. A simplified version of [16] is presented in [17] based on a model predictive technique.

In the second approach [3], [7], [19], [20], a simple PI controller is used to regulate the capacitor voltage, while vector control of the motor is also implemented using PI controllers. In addition to this, a separate PI controller is used to operate the main bridge (MB) at unity power factor to maximize the

Manuscript received June 15, 2019; revised September 20, 2019; accepted November 8, 2019. Date of publication November 20, 2019; date of current version March 13, 2020. This work was supported by the University of Alberta FES Initiative under Project T06-P01 "Smart Grids Structures." Recommended for publication by Associate Editor D. G. Xu. *(Corresponding author: Chatumal Perera.)*

The authors are with the Department of Electrical and Computer Engineering, University of Alberta, AB T6G 2W3, Canada (e-mail: sachindr@ualberta.ca; gkish@ualberta.ca; john.salmon@ualberta.ca).

Color versions of one or more of the figures in this article are available online at http://ieeexplore.ieee.org.

Digital Object Identifier 10.1109/TPEL.2019.2955412

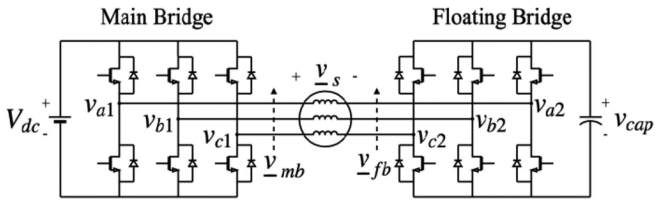

Fig. 1. DID with floating capacitor bridge using OEWIM.

operating range of the drive. The advantage of this approach is its simplicity of implementation with respect to the first approach. Also, this approach is not limited to a specific inverter dc-link voltage ratio. This fact has been exploited in [7] and [20] where a variable floating bridge (FB) dc-link voltage has been used to improve the efficiency of the system through constant power factor operation and by reducing FB losses, respectively.

This article improves upon the control scheme presented by the authors in [21] which also uses a PI controller to regulate the capacitor voltage. The contribution of this article is twofold.

1) A control scheme for the DID that practically decouples the motor and capacitor dynamics even for small FB capacitance values. It is extensively demonstrated via simulations and experiments that the capacitor voltage can be kept constant even during large step changes in the motor speed reference (0 to 1 pu) and load torque (0.25 to 0.75 pu). Only voltage switching ripple variation is observed. As a result, a significantly smaller (more than 10 times smaller compared to previous works) FB capacitor can be used for the same switching frequency and output power. This also allows for the use of thin film capacitors which have higher reliability and lower parasitics compared to electrolytic capacitors. A guideline for choosing the capacitor size is also provided.
2) The above benefit is realized by the use of a stator current reference frame. This reference frame is revealed to decouple the voltage requirements of the motor and FB capacitor into their real and reactive power components. Consequently, true decoupling of motor and capacitor dynamics can be realized. Also, the need for the dedicated PI controller used in [3], [19], [20] to operate the MB at unity power factor is eliminated, further simplifying the control. This allows the MB to supply part of the reactive power requirement of the motor during low torque operation, which reduces the dc-link voltage requirements.

II. Principles of Operation

The schematic of a DID with a floating capacitor bridge using an OEWIM is shown in Fig. 1. The main inverter bridge dc-link is connected to a dc source while the floating inverter bridge dc-link is connected to a capacitor. One end of each motor winding is connected to the MB, while the other end is connected to the FB. It is evident that there is no path for common mode currents which produce losses. Also, the use of only one dc source cuts down on the cost, size, and weight of the drive, as opposed to using two isolated dc sources. The drive can also provide an additional reactive voltage boost without having to increase the input dc-voltage requirement of the drive. The effective line voltage seen by the motor can have up to 5-levels [9]. This reduces both the motor current distortion and PWM harmonic volt seconds, which in turn reduces the copper and iron losses in the motor.

The motor is controlled by manipulating its effective stator voltage $\underline{v}_s$ which is given by (1). $\underline{v}_s$ is equal to the difference between the MB output voltage SV $\underline{v}_{mb}$ and the FB output voltage SV $\underline{v}_{fb}$

$$\underline{v}_s = \underline{v}_{mb} - \underline{v}_{fb}. \tag{1}$$

The FB is mainly used to provide reactive voltage support. Hence, $\underline{v}_{fb}$ will nominally be 90° out of phase with the motor current at steady state. However, due to losses in the capacitor in a practical system, the capacitor will discharge over time and lose voltage. To counter this, a small component of $\underline{v}_{fb}$ is kept in phase with motor current to absorb real power and compensate for the losses. This component can be used to charge or discharge the capacitor as required.

Since the MB is the only source of real power, the output power rating of the drive will depend on the real power output of the MB. To maximize this, the power factor of the MB is maintained at unity over the whole operating range with a PI controller in previous works [3], [19], [20]. The need for this PI controller is eliminated in this aritcle using a stator current reference frame. We shall also show that unity power factor operation of the MB to maximize output power capability is only required at high torque operation at rated speed. The MB can be used to supply some reactive power during low torque operation at rated speed and support the FB. This can be used to reduce the dc-link voltage requirements.

III. Proposed Control Scheme

The main feature of the proposed control scheme is its ability to practically decouple the motor and capacitor dynamics even for a small capacitance value. This has the effect that the capacitor voltage can be kept constant during large step changes in motor speed reference and load torque. This allows for the use of a smaller FB capacitor to reduce the drive footprint. A key aspect enabling this is the use of the stator current reference frame (SCRF) [22] and the manner in which voltage references for each inverter bridge is set. This greatly simplifies the control and eliminates the need for a separate PI controller to operate the MB at unity power factor. During low torque (low power factor operation), the MB is allowed to supply some reactive power and support the FB, which reduces the dc-link voltage requirements. The objectives of the control scheme are listed below:

1) control the speed of the motor;
2) regulate the FB capacitor voltage;
3) operate the MB at unity power factor during high torque operation to maximize output power capability and supply reactive power if needed during low torque operation.

The first objective may be achieved by controlling the motor torque using vector control [18] which uses the rotor flux reference frame (RFRF). The q-axis current controls the motor torque while the d-axis current controls the motor flux. An outer speed

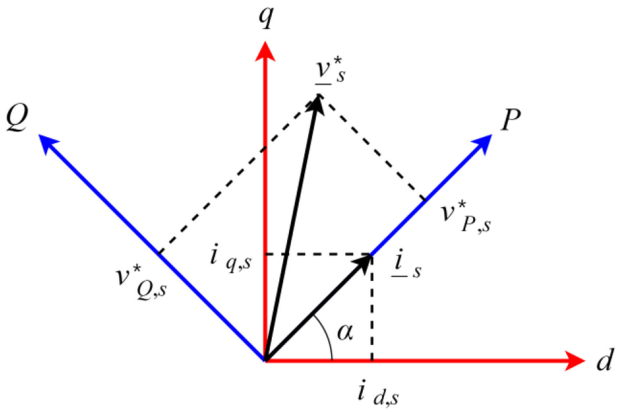

Fig. 2. Conversion of stator voltage from rotor flux reference frame to stator current reference frame.

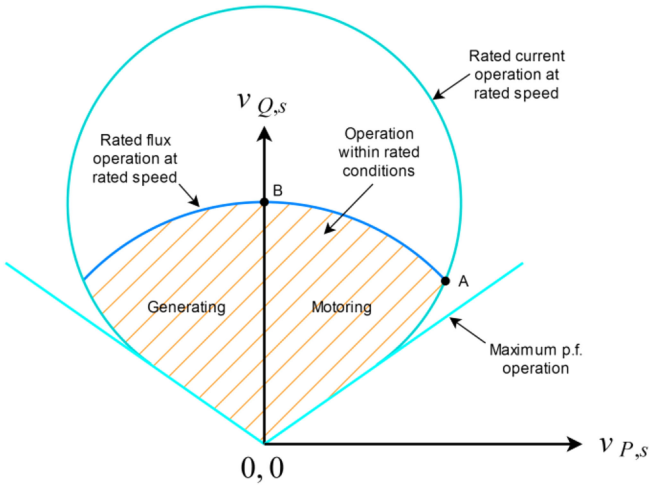

Fig. 3. Operating voltage range of an IM in the *PQ*-voltage plane (SCRF).

control loop is used to provide the *q*-axis current reference to the inner current control loop. The *d*-axis current reference is held constant at the rated value to maintain rated flux. Alternatively, the *d*-axis current may be set by a field weakening outer control loop as in [3], [19], [20], if operation above the rated speed is required. The second control objective is achieved by controlling the real power flow into the FB, while the third objective is achieved by keeping the reactive power output of the MB at zero during high torque operation.

A. Stator Current Reference Frame

It is clear that control objectives 2 and 3 listed above require the ability to control the real and reactive power outputs of the two inverter bridges. To do this, the real and reactive voltage components required by the motor need to be decoupled. The RFRF used in vector control is not very useful in this sense, since it only decouples the torque and field components of the stator current. However, by using the SCRF, as shown in Fig. 2, the motor voltage may be decoupled into its real and reactive components. In this reference frame, the *P*-axis is set to align with the stator current SV $\underline{i}_s$, while the *Q*-axis is set to lead $\underline{i}_s$ by 90°. Any voltage component along the *P*-axis will cause a real power transfer since it is in phase with the current, while any voltage component along the *Q*-axis will produce a reactive power transfer. The *P*-axis of the SCRF will lead the *d*-axis of the RFRF by an angle α. Hence, the position θ_{current} of the *P*-axis with respect to time is given by

$$\theta_{\text{current}} = \theta_{\text{flux}} + \alpha \tag{2}$$

$$\alpha = \tan^{-1}\left(i_{q,s}/i_{d,s}\right) \tag{3}$$

where θ_{flux} is the position of the *d*-axis of the rotor flux synchronous reference frame with respect to time. It should be clear that the *P*-axis component $i_{P,s}$ of current SV $\underline{i}_s$ is equal to the magnitude of the stator current $|\underline{i}_s|$, while the *Q*-axis component $i_{Q,s}$ is equal to zero.

The use of the RFRF of vector control is required only up to the point where the stator voltage reference $\underline{v}^*_s$ is calculated by the *dq*-axis current control loop. Once the components of $\underline{v}^*_s$ are calculated in the RFRF (*dq*-axis), they can be easily converted to the SCRF (*PQ*-axis) using the simple linear transformation given by (4). $v^*_{P,s}$ will correspond to the real power requirement of the motor while $v^*_{Q,s}$ corresponds to the reactive power requirement. Having these components decoupled will prove to be greatly useful when assigning output voltage references, as will be shown later

$$\begin{pmatrix} v^*_{P,s} \\ v^*_{Q,s} \end{pmatrix} = \begin{pmatrix} \cos\alpha & \sin\alpha \\ -\sin\alpha & \cos\alpha \end{pmatrix} \begin{pmatrix} v^*_{d,s} \\ v^*_{q,s} \end{pmatrix}. \tag{4}$$

Any other quantity including motor current may be converted to the SCRF from the RFRF by multiplying the *dq*-axis quantities by the rotation matrix used in (4) above.

The stator voltage requirement of the IM in the SCRF is shown in Fig. 3. The stator voltage will always fall in the shaded region if the IM is operated within rated conditions. This region is bounded by the rated current and flux limits at rated speed and the maximum power factor capability of the machine. The operation of the motor at rated flux and rated speed is shown by curve segment AB, which gives the maximum voltage requirement of the motor and determines the dc-link voltage requirements. Point A corresponds to rated torque operation at rated flux and speed where the *P*-axis voltage requirement is maximum. As the torque of the motor decreases, the operation point moves along AB to the left, reducing the *P*-axis requirement while increasing the *Q*-axis requirement. Hence, the power factor of the motor decreases. Point B corresponds to no load operation at rated flux and speed where the *Q*-axis requirement is maximum, and the power factor is minimum.

B. Capacitor Voltage Control

The FB capacitor voltage v_{cap} is governed by the following differential equation:

$$\frac{d}{dt}v_{\text{cap}} = \frac{i_{\text{cap}}}{C} = \frac{1}{C}\left(\frac{3}{4}m_{P,fb}\cdot i_{P,s} - i_{\text{loss,cap}} - i_{\text{PWM}}\right). \tag{5}$$

According to (5), v_{cap} is controlled by manipulating the capacitor current i_{cap}. During the start-up of the drive, i_{cap}

is kept positive to charge up the capacitor until it reaches the required voltage. Once it reaches this voltage, the capacitor voltage is kept constant by keeping the average of $i_{\rm cap}$ equal to zero. It is clear from (5) that $i_{\rm cap}$ consists of three components. The first component is due to the real power exchange at the fundamental frequency on the ac side of the FB inverter. This is proportional to the product of $i_{P,s}$ and the *P*-axis component of the FB inverter modulation index defined below

$$m_{P,fb} = v^*_{P,fb}/\left(v_{\rm cap}/2\right) \tag{6}$$

where $v^*_{P,fb}$ is the *P*-axis component of the FB voltage reference. The second component $i_{\rm loss,cap}$ models the power loss in the capacitor due to parasitic effects. The third component $i_{\rm PWM}$ models the real power exchanged due to the interaction of the high frequency PWM voltage and current components. It must be noted here that $i_{\rm PWM}$ is low frequency (dc at steady state) with a nonzero average representing power exchange. The value of $i_{\rm PWM}$ may be either positive or negative and varies with the operating conditions of the drive.

It is clear from (5) that $m_{P,fb}$ is the only control variable in the equation while $i_{P,s}$, $i_{\rm loss,cap}$, and $i_{\rm PWM}$ are disturbances. $v_{\rm cap}$ is maintained constant by adjusting $m_{P,fb}$ via a PI controller. The terms $i_{P,s}$ and $i_{\rm PWM}$ are highly sensitive to changes in motor operating conditions. Hence, the bandwidth of the PI controller should be fast enough to react to step changes in these values. The effect of $i_{P,s}$ can be reduced by feedforwarding it. However, $i_{\rm PWM}$ is very hard to predict or measure and can only be negated through the controller. Typically, a bandwidth of a few hundred hertz (∼200 Hz) is sufficient to decouple the effects of motor transients on $v_{\rm cap}$ for all practical purposes. What is meant by this is that the disturbance in $v_{\rm cap}$ will be smaller than the steady-state ripple making it unnoticeable.

C. Inverter Voltage Reference Assignment

The assignment of inverter voltages must be done such that the control requirements of the motor and the capacitor voltage do not interfere with each other. The real voltage component of the FB voltage reference $v^*_{P,fb}$ is reserved for controlling $v_{\rm cap}$ according to (5) by adjusting $m_{P,fb}$. $m_{P,fb}$ is usually very small (∼±0.1), allowing the rest of the FB voltage capability to be used for supplying reactive voltage. The reactive component of the FB voltage has no effect on $v_{\rm cap}$ and can be set arbitrarily. Hence, this component can be set to supply as much of the reactive voltage requirement of the motor as possible. The FB voltage reference $\underline{v}^*_{PQ,fb}$ can thus be assigned as follows

$$\underline{v}^*_{PQ,fb} = \begin{pmatrix} m_{P,fb}\left(v_{\rm cap}/2\right) \\ -{\rm sat}\left(v^*_{Q,s}\right) \end{pmatrix} \tag{7}$$

where

$${\rm sat}\left(v^*_{Q,s}\right) = \begin{cases} v^*_{Q,s}, & \text{if } v^*_{Q,s} \le v_{Q{\rm max},fb} \\ v_{Q{\rm max},fb}, & \text{otherwise.} \end{cases} \tag{8}$$

The *P*-axis component in (7) is equal to the real voltage component needed to keep $v_{\rm cap}$ constant. The *Q*-axis component is set to be equal to the reactive voltage requirement of the motor given that it is less than a predefined *Q*-axis saturation limit $v_{Q{\rm max},fb}$ (eg: $0.95v_{\rm cap}/2$ or $1.1v_{\rm cap}/2$). The dc-link voltage of the FB should be chosen high enough so that it is able supply $v^*_{Q,s}$ without saturating when the real power requirement of the motor is high. For example, when the motor is running at rated torque at rated speed. This allows the MB to operate at unity power factor, maximizing the output power capability of the drive. If $v^*_{Q,s}$ is larger than the saturation limit (eg: during low torque operation), the FB will only supply the saturation limit voltage while the remainder of $v^*_{Q,s}$ will be supplied by the MB.

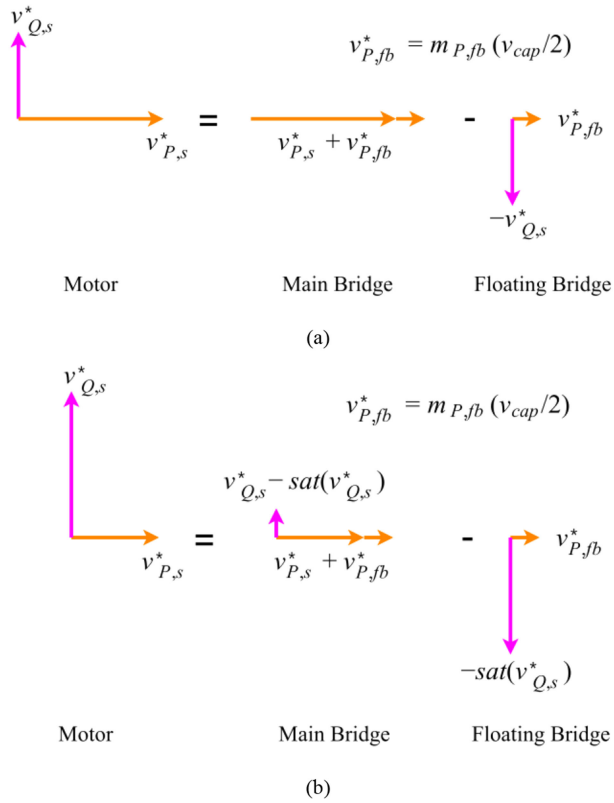

Fig. 4. Voltage references for motor, main bridge and floating bridge during rated speed operation at (a) high (close to rated) torque and (b) low torque.

The MB is the only source of real power and must supply both the real voltage component of the motor $v^*_{P,s}$, and the real voltage component of the FB $m_{P,fb}(v_{\rm cap}/2)$. It will also supply any remainder of $v^*_{Q,s}$ that the FB is unable to supply by itself. Thus, the MB voltage reference $\underline{v}^*_{PQ,mb}$ can be assigned as follows:

$$\underline{v}^*_{PQ,mb} = \begin{pmatrix} v^*_{P,s} + m_{P,fb}\left(v_{\rm cap}/2\right) \\ v^*_{Q,s} - {\rm sat}\left(v^*_{Q,s}\right) \end{pmatrix}. \tag{9}$$

When the real voltage requirement of the motor is maximum, i.e., when the motor is operating at rated speed at rated torque, the FB will supply the whole $v^*_{Q,s}$ requirement. Hence, $v^*_{Q,s} - {\rm sat}(v^*_{Q,s}) = 0$ and the MB will operate at unity power factor, maximizing the output power capability of the drive [Fig. 4(a)]. Note that a separate PI controller is not needed to do this as in previous works, making the proposed scheme simpler. For lower torque operation, the real voltage requirement

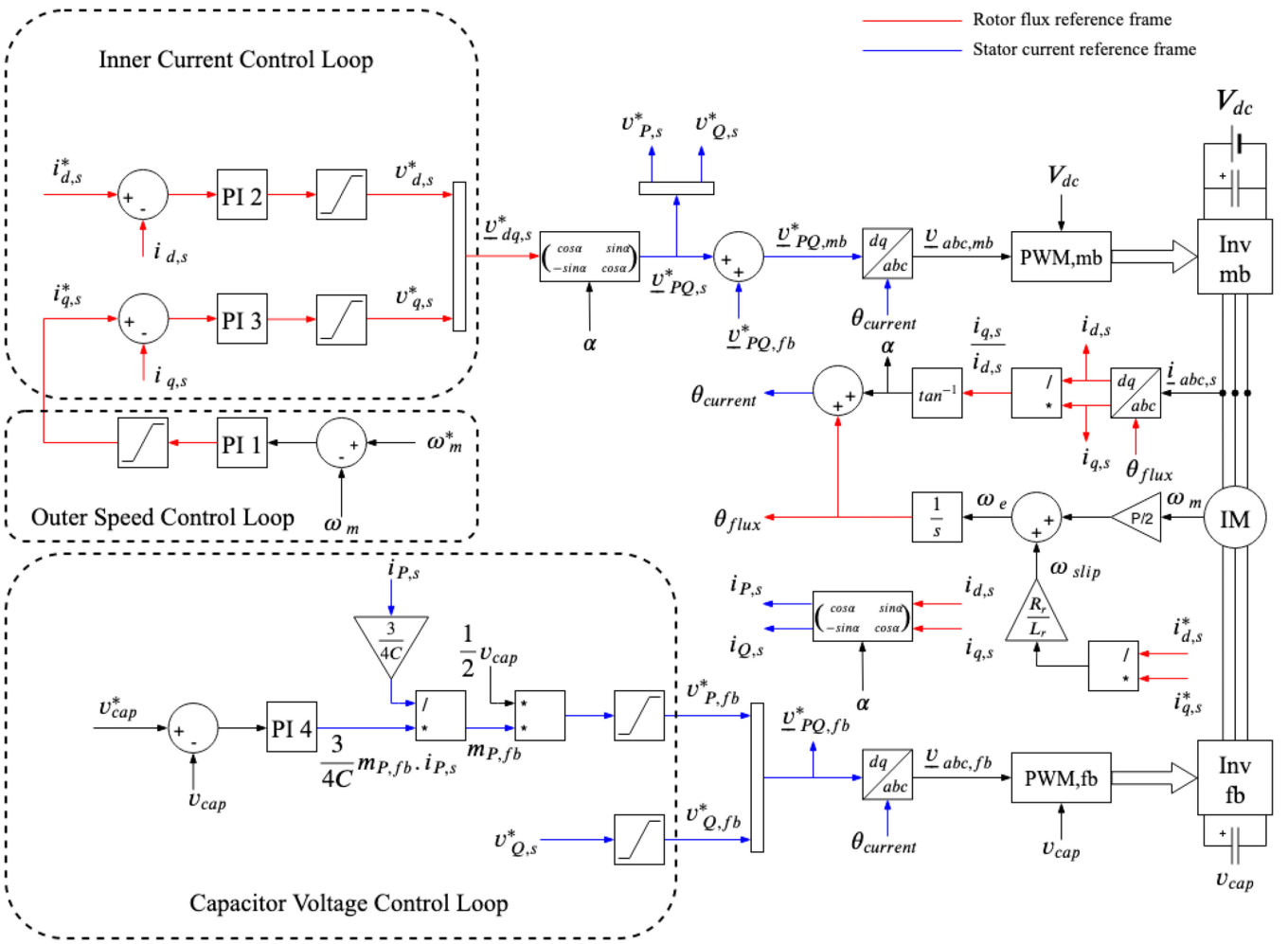

Fig. 5. Block diagram of the proposed control scheme for the DID with a floating capacitor bridge using an OEWIM.

of the motor will decrease while the reactive voltage requirement increases. The MB is then used to supply the remaining reactive voltage component $(v_{Q,s}^* - \mathrm{sat}(v_{Q,s}^*))$ which the FB cannot supply [Fig. 4(b)]. Thus, the dc-link voltage requirements can be reduced. This is the main difference between the proposed scheme and the scheme in [21] which always operates the MB at unity power factor by setting $v_{Q,mb}^* = 0$.

The voltage seen by the stator of the motor when the inverter voltage references are set according to (7) and (9) is given by

$$\underline{v}_{PQ,s} = \underline{v}_{PQ,mb}^* - \underline{v}_{PQ,fb}^* = \begin{pmatrix} v_{P,s}^* \\ v_{Q,s}^* \end{pmatrix}. \tag{10}$$

It can be seen that $\underline{v}_{PQ,s}$ is exactly equal to the stator voltage reference provided by the current control loop and contains no terms related to the FB voltage. Hence, the motor will be not be affected by the dynamics of the capacitor and can be controlled independently. Similarly, since the P-axis component in (7) is solely set by the PI controller for v_{cap}, independent control of v_{cap} is also achieved. This decoupling and simplicity are both results of the use of the SCRF. The proposed control scheme block diagram is shown in Fig. 5. The signals in the RFRF are shown in red, while the signals in the SCRF are shown in blue. Simple carrier-based PWM with third harmonic injection is used for the modulation of both inverters.

TABLE I
CONTROLLER GAIN SELECTION

Controller	Bandwidth (Hz)	k_P	k_I
Speed	10	0.9	16.96
i_d	150	46.36	$2.913\text{x}10^4$
i_q	150	46.36	$2.913\text{x}10^4$
v_{cap}	300	0.3	18.85

D. Controller Gain Selection

The bandwidths of the different controllers used and their corresponding k_P and k_I values are listed in Table I. The bandwidth of d- and q-axis current controllers were chosen to be 150 Hz. The outer speed control loop was set to have a bandwidth of 10 Hz. As mentioned in Section III-B, the capacitor voltage

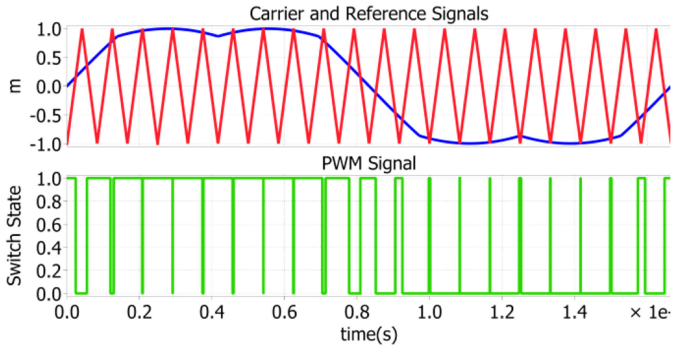

Fig. 6. Modulation scheme demonstrated for a single phase.

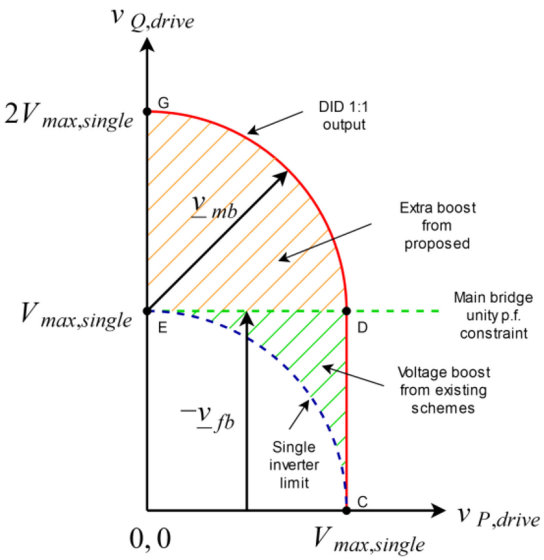

Fig. 7. Extra voltage boost from a 1:1 DID due to proposed scheme compared to always operating the main bridge at unity power factor.

control typically requires a bandwidth of around 200 Hz for decoupled dynamics. Hence, the bandwidth of this controller was selected to be 300 Hz.

E. Modulation Scheme

The inverters are modulated independently of each other using carrier-based modulation with third harmonic injection. Hence, the modulation scheme is not limited to the 1:1 dc-link ratio used in this article and can be used with a 2:1 or 1:2 ratio if required. The scheme is also simple to implement and allows each inverter to operate at a maximum modulation index of 1.15. The same carrier signal is used to modulate all six reference signals of the different phases. The manner in which each phase is modulated is shown in Fig. 6.

F. Extra Voltage Boost and Reduction of dc-link Voltages

The voltage boost obtained from the proposed scheme due to the MB supplying part of the reactive voltage requirement at low power factor (low torque) operation is shown in Fig. 7. CDE is the maximum output voltage capability of a 1:1 DID

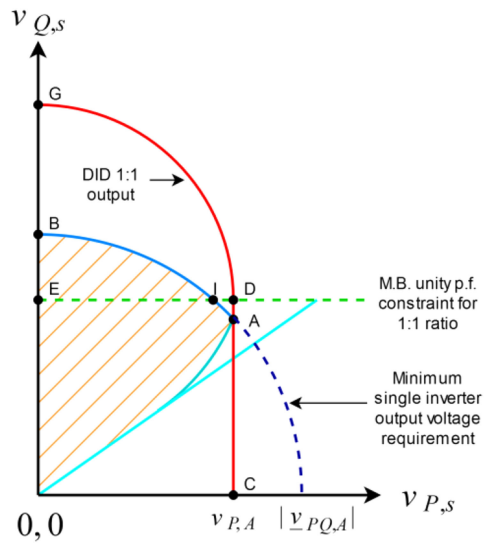

Fig. 8. Minimum 1:1 DID voltage requirement.

operating the MB at unity power factor, while CDG is the maximum capability of the proposed scheme. Note that $\underline{v}_{mb}$ must be horizontal for unity power factor operation while there is no such constraint for the proposed scheme. This results in the extra voltage boost shown by portion GDE for the proposed scheme. The proposed scheme can double the reactive voltage capability of a 1:1 DID at low power factor (point G Fig. 7). DID dc-links are usually chosen in ratios such as 2:1 [16], [17], and [5], 1:1 [9], [21] or 1:2 [3] to improve PWM quality.

The minimum output voltage requirement for a 1:1 DID is shown in Fig. 8 by superimposing the DID voltage capability curve of Fig. 7 on the motor voltage requirement curve of Fig. 3. The minimum dc-link voltage should be chosen such that the DID can supply the voltage within the shaded region. For the proposed scheme using a 1:1 dc-link, this means that the dc-link voltage is determined by the *P*-axis (real) voltage requirement $v_{P,A}$ of point A. Point A corresponds to the operation of the motor at rated torque and speed. The minimum dc-link voltages needed for a 1:1 DID using the proposed scheme is thus given by

$$V_{\mathrm{DC},mb} = V_{\mathrm{DC},fb} = \frac{2 \cdot v_{P,A}}{\eta} = \frac{2\sqrt{2}}{\sqrt{3}\eta} v_{\mathrm{rms}} \cos\varphi_{\mathrm{rated}} \quad (11)$$

where v_{rms} and $\cos\varphi_{\mathrm{rated}}$ are the rms line voltage and power factor of the motor at rated conditions. η is a derating factor typically chosen to be in the range 0.9–0.95. If unity power factor operation of the MB is used, the dc-link voltage given by (11) would be insufficient to operate the motor in region BIE (Fig. 8) which corresponds to low power factor operation. Hence, the dc-link voltage for unity power factor operation of the MB is determined by point B (no load operation at rated speed). Either both dc-links must be increased if a 1:1 ratio is used, or the FB dc-link should be doubled while keeping the MB link at (11) to give a 1:2 ratio.

Table II compares the dc-link voltage requirements for unity power factor operation of the MB, and for the proposed scheme

TABLE II
COMPARISON OF MINIMUM SUPPLY VOLTAGE REQUIREMENT AT $\eta = 0.95$ FOR DIFFERENT DRIVE CONFIGURATIONS FOR A 230-V MOTOR

Drive Configuration	MB DC Link Voltage (V)	FB DC Link Voltage (V)
DID 1:1 DC link ratio, unity PF operation MB	397	397
DID 1:2 DC link ratio, unity PF operation MB	295	590
DID 1:1 DC link ratio, proposed control	295	295

to drive a 230-V motor at $\eta = 0.95$. The proposed scheme can reduce both the MB and FB dc-link voltages by 26% to 295 V compared to a 1:1 DID operating the MB at unity power factor. However, reducing the MB dc-link voltage is more important compared to the FB, since it is the input supply voltage to the drive. The same supply voltage of 295 V can be used for MB unity power factor operation if a 1:2 dc-link ratio is used. But the FB dc-link voltage must be doubled compared to the proposed scheme. Hence, using the proposed scheme with a 1:1 DID is beneficial in terms of component voltage ratings. Additionally, the design process of the drive will be simplified since both inverters will have identical specifications.

G. Potential Operation in Field Weakening Region

Extension of the speed range in the field weakening region is one of the advantages of the DID [3]. However, the focus of this article was decoupling motor and capacitor dynamics and reducing capacitor size. The proposed scheme may be modified to incorporate field weakening by adding an outer control loop to adjust the *d*-axis current reference of the current controller in a manner similar to [3].

The extra voltage boost GDE (Fig. 7) provided by the proposed scheme does however give a potential advantage for operation in the field weakening region. It has been shown in [3] that the upper limit $\omega_{\rm pow}$ of the constant power region (field weakening region I) can be extended to (12) by using a DID

$$\omega_{\rm pow} \approx |\underline{v}_{fb,\max}| \,/\, (\sigma L_s I_{s,\max}) \tag{12}$$

where $\underline{v}_{fb,\max}$ is the maximum output voltage capability of the FB, σ is the leakage coefficient, and $I_{s,\max}$ is the rated value of the peak stator current. Equation (12) may be derived by considering the reactive voltage requirement of the motor at $\omega_{\rm pow}$ which is close to $\omega_{\rm pow}\sigma L_s I_{s,\max}$ and the maximum reactive voltage capability of the DID. If the MB is always operated at unity power factor, the reactive voltage capability of the DID will be $|\underline{v}_{fb,\max}|$, resulting in (12). However, for the proposed scheme, the reactive voltage capability is increased due to the MB being able to supply some reactive voltage which has the possibility of further increasing $\omega_{\rm pow}$.

IV. RESULTS

To demonstrate the effectiveness of the proposed scheme, the following two tests were performed.

1) *Test 1* – The motor is given a step in speed reference from 0 to rated speed (1760 rpm) at 0.25 pu (5 Nm) torque.
2) *Test2* – The motor is given a 0.5 pu (10 Nm) step in load torque from 0.25 pu (5 Nm) to 0.75 pu (15 Nm) at rated speed (1760 rpm).

Both tests represent extreme transients in motor operating conditions. These tests were performed both in simulation and experimentally. The same motor and drive parameters were used in the simulation and experiment. These values are given in Table III.

TABLE III
DID SYSTEM PARAMETERS

Parameter	Symbol	Value
Stator resistance	R_s	0.466 Ω
Rotor resistance	R_r	0.2873 Ω
Stator leakage inductance	L_{ls}	3.03 mH
Rotor leakage inductance	L_{lr}	2.02 mH
Magnetizing inductance	L_m	47 mH
Number of poles	p	4
Rated power	P_{rated}	5 hp
Rated speed	N_{rated}	1760 rpm
Rated torque	T_{rated}	20 Nm
Moment of inertia	J	0.0279 kg m^2
Coefficient of friction	B	6.41x10^{-4} kg m^2 s^{-1}
Rated current	I_{rms}	13.6 A
Rated line voltage	V_{rms}	230 V
Floating bridge capacitance	C	120 µF
Main DC link voltage	$V_{DC,mb}$	300 V
Floating DC link voltage	$V_{DC,fb}$	300 V
Switching frequency	f_s	5 kHz

A. Simulation Results

The two tests mentioned above were performed on the DID system and the waveforms of the four parameters being controlled ($i_{d,s}$, $i_{q,s}$, motor speed, and $v_{\rm cap}$) were plotted.

The waveforms corresponding to *Test 1* are shown in Fig. 9. The behavior of $i_{d,s}$, $i_{q,s}$, and the motor speed is the same as what would be expected from a single inverter drive. Hence, it can be concluded that the motor dynamics are not affected by the FB control requirements. The motor accelerates from 0 to rated speed (1760 rpm) in less than 300 ms. However, the most important observation is that the capacitor voltage remains constant despite of this large motor transient. The only observable change is the increase in capacitor voltage ripple. This shows that the proposed scheme is able to decouple the capacitor dynamics from the motor dynamics as claimed.

The waveforms for *Test 2* are shown in Fig. 10. Again, the behavior of $i_{d,s}$, $i_{q,s}$, and the motor speed is the same as what would be expected from a single inverter drive. The motor speed drops slightly by about 40 rpm with the step in load torque but quickly recovers within 250 ms. More importantly, the capacitor voltage remains constant despite the step in load torque. Once again, this confirms the ability of the proposed scheme in decoupling motor and capacitor dynamics. Fig. 10(d) shows the inverter voltage references in the *PQ*-reference frame. Before the step in load torque, the motor is operating in the low torque region where the *Q*-axis (reactive) voltage requirement of the motor is higher than what the FB can supply. Hence, the FB *Q*-axis reference saturates at -165 V ($-v_{Q\max,fb}$ limit) while the MB supplies the remainder of the *Q*-axis requirement.

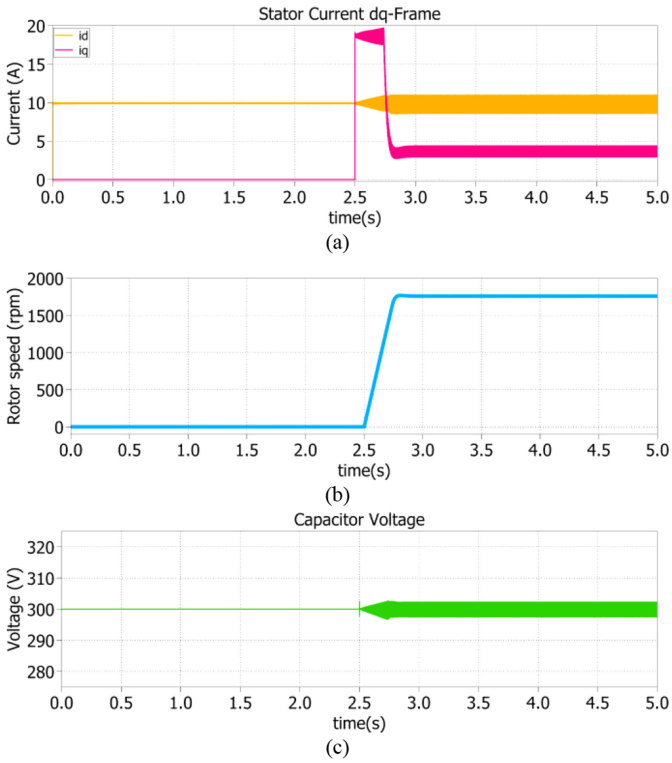

Fig. 9. Simulated dynamic response of controlled parameters during a step in speed reference from 0 to rated speed (1760 rpm) at 0.25 pu (5 Nm) torque. (a) $i_{d,s}$ and $i_{q,s}$. (b) Motor speed. (c) $v_{\rm cap}$.

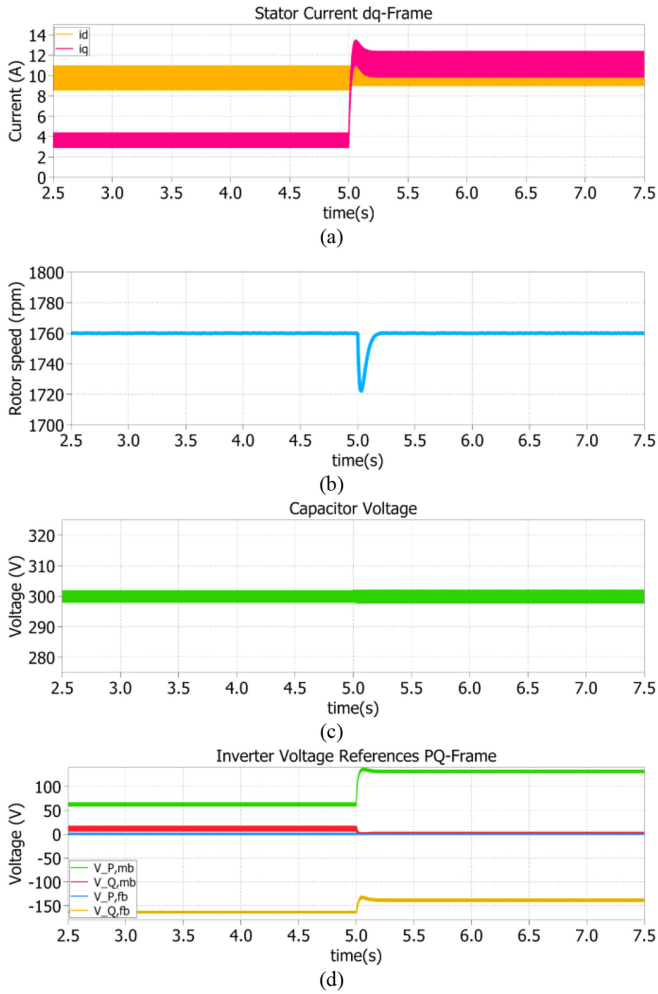

Fig. 10. Simulated dynamic response of controlled parameters during a 0.5 pu (10 Nm) step in load torque from 0.25 pu (5 Nm) to 0.75 pu (15 Nm) at rated speed (1760 rpm). (a) $i_{d,s}$ and $i_{q,s}$. (b) Motor speed. (c) $v_{\rm cap}$. (d) Inverter voltage references.

After the transient, the motor operates in the high torque region and the FB is able to supply the full Q-axis requirement of the motor alone. Therefore, the MB supplies zero Q-axis voltage and operates at unity power factor. Hence, the MB is able to supply reactive power when needed, allowing for reduced dc supply requirements compared to always operating the MB at unity power factor. A 300 V dc-link voltage was used for both the MB and FB, which was chosen just above the value given by (11) and Table II.

In addition to the results for *Test 1* and *Test 2*, Fig. 11 shows the simulated response of the controlled parameters during regeneration and reverse motoring. A step in speed reference was given from rated speed in the forward direction (1760 rpm) to rated speed in the reverse direction (-1760 rpm). The motor operates in the regenerating mode as its speed drops from 1760 to 0 rpm and in the reverse motoring mode as the speed increases in the reverse direction from 0 to -1760 rpm. Even under these conditions, the capacitor voltage remains constant at 300 V. The only observable change is the variation in voltage ripple, similar to the results observed in *Test 1* and *Test 2*.

B. Experimental Results

The same two tests mentioned above were repeated experimentally. The motor used was a 230 V, 5 hp, class B Baldor OEWIM. The DID consisted of two identical custom built inverters with Semikron (SKiM306GD12E4, 1200 V, 300 A) IGBT modules. Three KEMET C4AQLBW5400A3FK 40 μF 500 V polypropylene film capacitors connected in parallel were used to form the FB capacitance of 120 μF. The detailed specifications of the motor and the drive are available in Table III. The drive control was implemented on a PLECS RT Box platform. The motor was loaded using a MAGTROL DSP 6000 dynamometer. The experimental setup is shown in Fig. 12. The dynamic response of the controlled parameters for *Test 1* is shown in Fig. 13. The experimental response is very similar to the simulation with the motor reaching rated speed (1760 rpm) within 300 ms. More importantly, there is no visible deviation in the capacitor voltage [Fig. 13(b)]. The only visible change is the increase in capacitor voltage ripple.

The same can be said about the *Test 2* experimental waveforms shown in Fig. 14. They are very similar to the simulation waveforms. The motor speed dips slightly but recovers within 250 ms while the capacitor voltage remains constant the whole time. Hence, it should be clear that the decoupling of motor and capacitor dynamics in the proposed scheme can be realized experimentally.

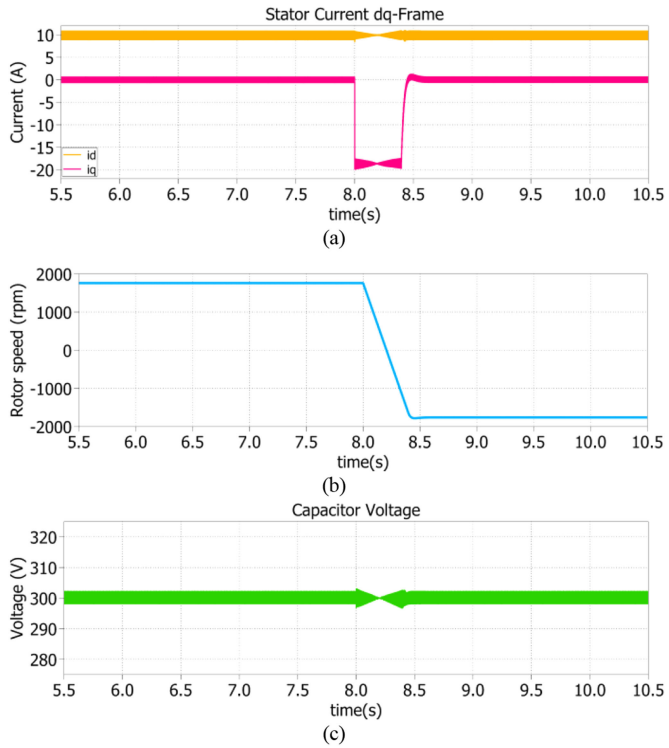

Fig. 11. Simulated dynamic response of controlled parameters during a step in speed reference from rated speed in forward direction (1760 rpm) to rated speed in reverse direction (−1760 rpm). (a) $i_{d,s}$ and $i_{q,s}$. (b) Motor speed. (c) $v_{\rm cap}$.

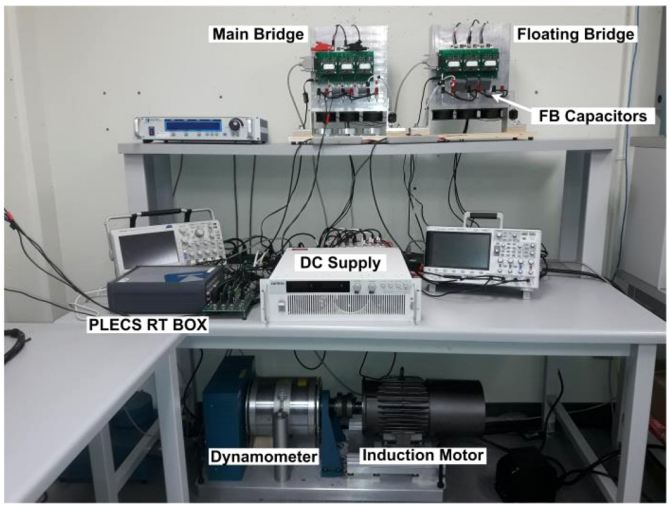

Fig. 12. Experimental setup.

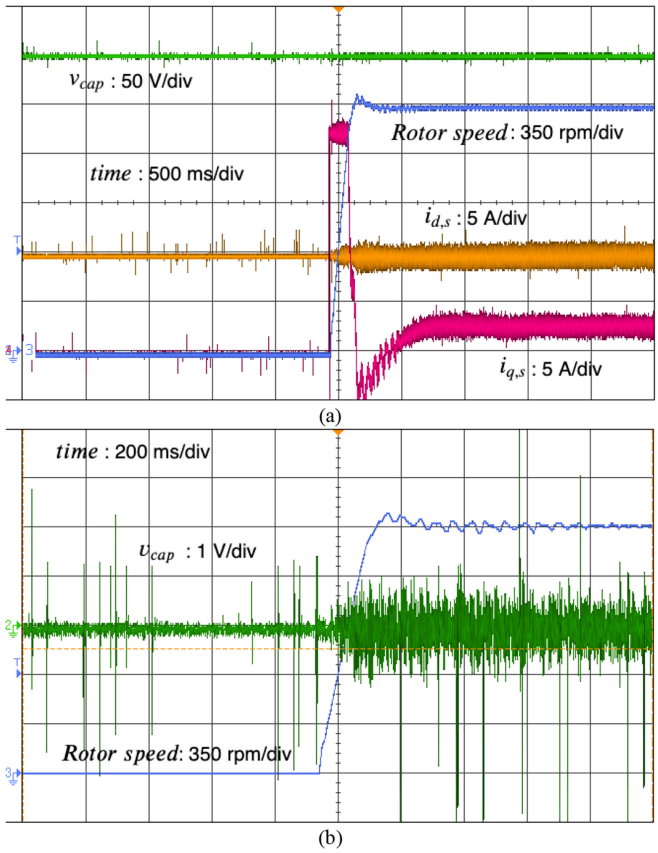

Fig. 13. Experimental dynamic response of controlled parameters during a step in speed reference from 0 to rated speed (1760 rpm) at 0.25 pu (5 Nm) torque. (a) All controlled parameters. (b) capacitor voltage zoomed.

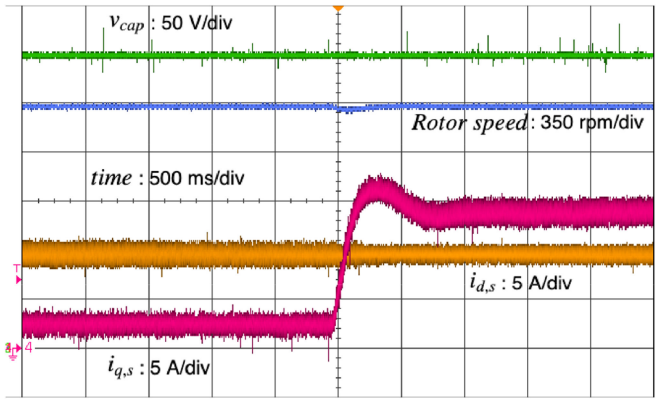

Fig. 14. Experimental dynamic response of controlled parameters during a 0.5 pu (10 Nm) step in load torque from 0.25 pu (5 Nm) to 0.75 pu (15 Nm) at rated speed (1760 rpm).

The reactive voltage support provided by the MB at rated speed during low torque operation is experimentally demonstrated in Fig. 15. As the load torque decreases, the power factor of the motor decreases and the reactive voltage requirement increases. At 5 Nm, the maximum reactive voltage capability of the FB is reached [Fig. 15(a)] and the MB starts supplying the remaining reactive voltage requirement. This is evident from the drop in power factor of the MB at torques below 5 Nm in Fig. 15(b). It is possible to do this since the MB is not running at its full capability during low torque operation. However, at higher torques, the MB operates at unity power factor close to its full capability.

The experimental plots for the motor voltage requirement over the whole torque range at different speeds is shown in Fig. 16. The leftmost point on each speed curve corresponds to no load operation while the rightmost point corresponds to rated torque operation. The portion of the curve at rated speed going above the MB unity power factor constraint corresponds to the operation at

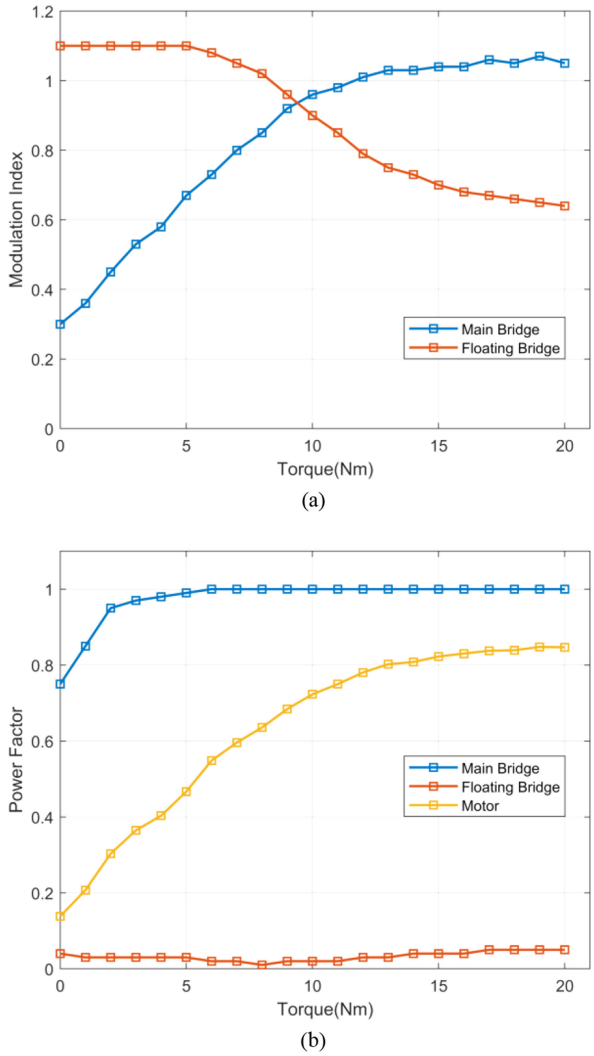

Fig. 15. Experimental variation. (a) Modulation Index. (b) Power Factor with load torque at rated speed (1760 rpm).

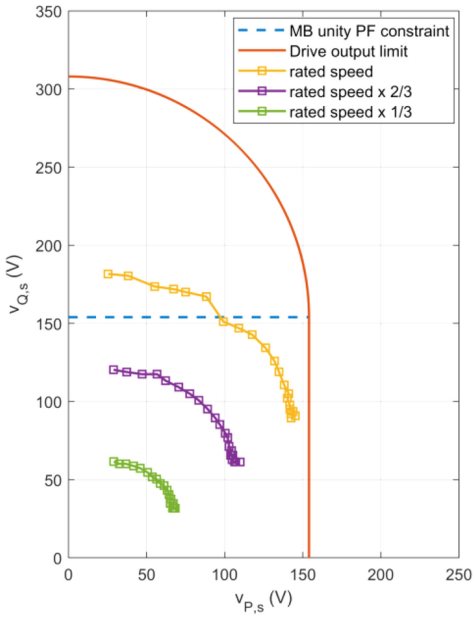

Fig. 16. Experimental motor voltage requirement in the *PQ*-voltage plane (SCRF) over the whole torque range at different speeds.

TABLE IV
COMPARISON OF FB CAPACITOR SIZES OF DIFFERENT OEWIM DID SCHEMES

Scheme	Capacitor control method	Experimentally demonstrated P_{max} (W)	f_s (kHz)	C (μF)	$\frac{Cf_s}{P_{max}}$ (μF.Hz/W)
Proposed	PI	3686	5	120	**163**
[3]	PI	690	NS	NS	-
[7]	PI	3686	7.5	4000	8139
[16]	PWM	1833	2	3250	3546
[17]	PWM	1833	3	3250	5319
[18]	PWM	7676	5	3250	2117
[21]	PI	1602	5	NS	-

NS = Not Specified

torques below 5 Nm where the MB supplies reactive voltage. At lower speeds however, the voltage requirement remains below the MB unity power factor constraint. Hence, the MB operates at unity power factor over the whole torque range for these speeds. Fig. 16 also experimentally validates Fig. 8 given earlier. The rated speed curve in Fig. 16 corresponds to line segment AIB in Fig. 8.

C. Selection of Floating Bridge Capacitor

Table IV shows a comparison of FB capacitor sizes and power levels between the proposed scheme and existing control schemes in literature. Please note that the values in column 3 have been inferred from the experimental speed and torque waveforms presented in these works and may not have been explicitly stated by the authors. These values have been listed only to provide an approximate feel regarding the system power level for the sake of comparison.

It is evident that all schemes listed in Table IV including the proposed scheme fall under the same power range (<10 kW) and use similar switching frequencies. However, the capacitor value used in the proposed scheme is an order of magnitude (more than 20 times) smaller than the next smallest capacitor size used. For a fairer comparison, the capacitor size has been normalized with respect to switching frequency and output power in the last column of Table IV to give the μF.Hz/W value for each scheme. It has been shown in [23] that the capacitance required is inversely proportional to f_s, indicating that it is easier to reduce C at higher f_s. This is why C is multiplied by f_s to get the normalized value instead of dividing by it. For example, if two schemes use the same C but one of them uses half the f_s as the other, it will have half the μF.Hz/W value, indicating it is twice as better. Even with this metric, the proposed scheme (163 μF.Hz/W) is an order of magnitude (more than 10 times) better with respect to capacitor size than the next closest scheme (2117 μF.Hz/W). This shows the effectiveness of the proposed scheme in reducing capacitor size.

The FB capacitance for the proposed scheme has been selected based on the worst case steady state capacitor voltage ripple, which occurs when the motor is running at its rated

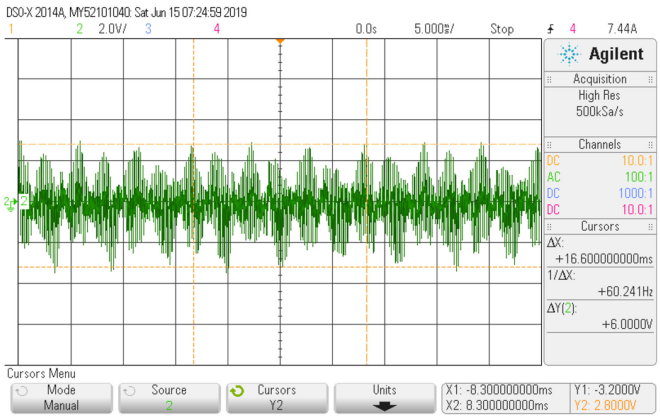

Fig. 17. Worst case experimental ripple voltage for $C = 120\ \mu$F and $f_s = 5$ kHz at rated torque (20 Nm) and rated speed (1760 rpm), timescale = 5 ms/div.

condition. The ripple is a result of the switching action of the FB inverter and is inversely proportional to capacitance. It is also proportional to the switched current flowing through the capacitor and the time for which it flows. The value of the switched current is related to the three phase motor currents. The time for which it is applied is equal to the dwell time of the switching state being applied, which is proportional to the FB voltage reference and inversely proportional to the switching frequency. Hence, the worst case ripple can be eventually related to capacitance, switching frequency and the rated parameters of the motor. Capacitance can be made the subject of this relation resulting in (13) which gives a guideline [23] for selecting the FB capacitance based on worst case peak to peak ripple $\Delta V_{\max}$, motor parameters and switching frequency f_s

$$C = \frac{V_{\rm rms} \cdot I_{\rm rms}}{2 \cdot V_{{\rm DC},fb} \cdot \Delta V_{\max} \cdot f_s} \sqrt{1 - \frac{1}{3}\left(\frac{P_{\rm rated}}{V_{\rm rms} \cdot I_{\rm rms}}\right)^2}. \quad (13)$$

The capacitance requirement predicted by (13) for a ripple of 6 V (2% of the FB dc-link voltage as in [5]), for the drive and motor parameters listed in Table III is 126 μF. Hence, the practical value of 120 μF was chosen for all simulations and experiments in this paper. The requirement of such a small capacitance value allows for the use of film capacitors which have much lower ESR and higher ripple current ratings compared to electrolytics. Hence, three KEMET C4AQLBW5400A3FK 40 μF, 500 V polypropylene film capacitors connected in parallel were used to form the required 120 μF. The maximum simulated rms ripple current through each capacitor was 2.1 A, which is much smaller than the rated value of 13.5 A for the selected capacitors. Hence, the value predicted by (13) is a practical value and is not limited by the capacitor ripple current rating. Fig. 17 shows the experimental ripple voltage obtained with the selected capacitors for the worst case scenario of rated torque at rated speed. As predicted, the ripple remains at 6 V (2%) which experimentally validates (13). The frequency of the ripple voltage (15 kHz) is 3 times the switching frequency due to the three phase switching action. Also, the amplitude of the switching ripple increases and decreases periodically at a frequency of 6 times the fundamental frequency (360 Hz). This is related to the existence of 6 sectors in the FB SV diagram [23].

V. Conclusion

A control scheme for the DID using an OEWIM with FB capacitor control has been proposed. The control scheme decouples the motor and capacitor dynamics such that the capacitor voltage can be kept constant even during large step changes in motor speed reference or torque for a capacitance as small as 120 μF. The proposed scheme is also simpler than existing schemes since it does not require a complex modulation scheme and uses only four PI regulators, only one more than a single inverter drive implementing vector control. Much of this simplicity is due to the use of the stator current reference frame and the manner in which voltage references are assigned to the inverters, which also allows the MB to supply some reactive power when required. This results in an additional voltage boost at low power factor operation compared to existing schemes, reducing dc-link voltage requirements. Both the MB and FB dc-link requirements can be reduced by 26% for a 1:1 DID, while the FB requirement can be cut by half compared to a 1:2 DID. Since the capacitor voltage is not affected by motor transients, the capacitor can be made very small and is selected based on steady-state ripple voltage. It also allows for the use of film capacitors which are more reliable and have lower parasitics compared to electrolytics. A guideline equation for the selection of capacitor size based on motor and drive parameters and ripple is provided. It is shown that the capacitance used by the proposed scheme is an order of magnitude smaller than any other scheme for the same switching frequency and output power.

Acknowledgment

We would like to thank Dr. S. Leng and A. Terheide for the support given in setting up the experimental setup.

References

[1] M. Zeraoulia, M. E. H. Benbouzid, and D. Diallo, "Electric motor drive selection issues for HEV propulsion systems: A comparative study," *IEEE Trans. Veh. Technol.*, vol. 55, no. 6, pp. 1756–1764, Nov. 2006.

[2] I. Boldea, L. N. Tutelea, L. Parsa, and D. Dorrell, "Automotive electric propulsion systems with reduced or no permanent magnets: An overview," *IEEE Trans. Ind. Electron.*, vol. 61, no. 10, pp. 5696–5711, Oct. 2014.

[3] M. Mengoni, A. Amerise, L. Zarri, A. Tani, G. Serra, and D. Casadei, "Control scheme for open-ended induction motor drives with a floating capacitor bridge over a wide speed range," *IEEE Trans. Ind. Electron.*, vol. 53, no. 5, pp. 4504–4514, Sep./Oct. 2017.

[4] H. Stemmler and P. Guggenbach, "Configurations of high-power voltage source inverter drives," in *Proc. 1993 5th Eur. Conf. Power Electron. Appl.*, Brighton, UK, 1993, vol. 5, pp. 7–14.

[5] Z. Huang, T. Yang, P. Giangrande, S. Chowdhury, M. Galea, and P. Wheeler, "An active modulation scheme to boost voltage utilization of the dual converter with a floating bridge," *IEEE Trans. Ind. Electron.*, vol. 66, no. 7, pp. 5623–5633, Jul. 2019.

[6] R. Shi, S. Semsar, and P. W. Lehn, "Constant current fast charging of electric vehicles via a DC grid using a dual-inverter drive," *IEEE Trans. Ind. Electron.*, vol. 64, no. 9, pp. 6940–6949, Sep. 2017.

[7] I. J. Smith and J. Salmon, "High-Efficiency operation of an open-ended winding induction motor using constant power factor control," *IEEE Trans. Power Electron.*, vol. 33, no. 12, pp. 10663–10672, Dec. 2018.

[8] M. Darijevic, M. Jones, O. Dordevic, and E. Levi, "Decoupled PWM control of a dual-inverter four-level five-phase drive," *IEEE Trans. Power Electron.*, vol. 32, no. 5, pp. 3719–3730, May 2017.

[9] C. Perera, G. J. Kish, and J. Salmon, "5-Level PWM scheme for a dual inverter drive using an open winding machine," in *Proc. 2018 IEEE Energy Convers. Congr. Expo.*, 2018, pp. 6975–6982.
[10] B. A. Welchko, T. A. Lipo, T. M. Jahns, and S. E. Schulz, "Fault tolerant three-phase AC motor drive topologies: a comparison of features, cost, and limitations," *IEEE Trans. Power Electron.*, vol. 19, no. 4, pp. 1108–1116, Jul. 2004.
[11] Y. Zhao and T. Lipo, "Space vector PWM control of dual three-phase induction machine using vector space decomposition," *IEEE Trans. Ind. Electron.*, vol. 31, no. 5, pp. 1100–1109, Sep. 1995.
[12] K. Sekhar and S. Srinivas, "Discontinuous decoupled PWMS for reduced current ripple in a dual two-level inverter fed open-end winding induction motor drive," *IEEE Trans. Power Electron.*, vol. 28, no. 5, pp. 2493–2502, May 2013.
[13] D. Wu, X. Wu, L. Su, X. Yuan, and J. Xu, "A dual three-level inverter-based open-end winding induction motor drive with averaged zero-sequence voltage elimination and neutral-point voltage balance," *IEEE Trans. Ind. Electron.*, vol. 63, no. 8, pp. 4783–4795, Aug. 2016.
[14] M. R. Baiju, K. K. Mohapatra, R. S. Kanchan, and K. Gopakumar, "A dual two-level inverter scheme with common mode voltage elimination for an induction motor drive," *IEEE Trans. Power Electron.*, vol. 19, no. 3, pp. 794–805, May 2004.
[15] A. Edpuganti and A. Rathore, "New optimal pulse width modulation for single dc-link dual-inverter fed open- end stator winding induction motor drive," *IEEE Trans. Power Electron.*, vol. 30, no. 8, pp. 4386–4393, Aug. 2015.
[16] S. Chowdhury, P. W. Wheeler, C. Patel, and C. Gerada, "A multilevel converter with a floating bridge for open-end winding motor drive applications," *IEEE Trans. Ind. Electron.*, vol. 63, no. 9, pp. 5366–5375, Sep. 2016.
[17] S. Chowdhury, P. W. Wheeler, C. Gerada, and C. Patel, "Model predictive control for a dual-active bridge inverter with a floating bridge," *IEEE Trans. Ind. Electron.*, vol. 63, no. 9, pp. 5558–5568, Sep. 2016.
[18] S.-K. Sul, "Vector Control [1 and 2]," in *Control of Electric Machine Drive Systems*, Piscataway, NJ, USA: IEEE Press, 2011, pp. 230–281.
[19] A. Amerise, M. Mengoni, L. Zarri, A. Tani, S. Rubino, and R. Bojoi, "Open-ended induction motor drive with a floating capacitor bridge at variable dc-link voltage," in *Proc. IEEE Energy Convers. Congr. Expo.*, 2017, pp. 3591–3597.
[20] A. Amerise, M. Mengoni, L. Zarri, A. Tani, S. Rubino, and R. Bojoi, "Open-End windings induction motor drive with floating capacitor bridge at variable DC-Link voltage," *IEEE Trans. Ind. Electron.*, vol. 55, no. 3, pp. 2741–2749, May/Jun. 2019.
[21] C. Perera, S. Leng, G. J. Kish, and J. Salmon, "Robust floating capacitor voltage control of dual inverter drive for open-ended winding induction motor," in *Proc. IEEE Appl. Power Electron. Conf. Expo.*, pp. 249–256.
[22] Z. Beres and P. Vranka, "Sensorless IFOC of induction motor with current regulators in current reference frame," *IEEE Trans. Ind. Electron.*, vol. 37, no. 4, pp. 1012–1018, Jul./Aug. 2001.
[23] C. Perera, G. J. Kish, and J. Salmon, "Guidelines for selecting minimum capacitance for a floating bridge dual inverter drive," in *Proc. IEEE Energy Convers. Congr. Expo.*, Baltimore, MD, USA, 2019, pp. 7064–7071.

Chatumal Perera (S'13) received the B.Sc.Eng. degree in electrical and electronic engineering (first-class hons.) from the Faculty of Engineering, University of Peradeniya, Galaha, Sri Lanka, in 2015. He is currently working toward the Ph.D. degree with the Department of Electrical and Computer Engineering, University of Alberta, Edmonton, AB, Canada.

His main research interests include PWM, induction motor drives and multilevel converters.

Gregory J. Kish (S'07–M'15) received the B.E.Sc. degree in electrical engineering from the University of Western Ontario, London, ON, Canada, in 2009, and the M.A.Sc. and Ph.D. degrees in electrical engineering from the University of Toronto, Toronto, ON, Canada, in 2011 and 2016, respectively.

He is currently an Assistant Professor with the University of Alberta, Edmonton, AB, Canada. His research interests include modular multilevel converters, HVDC, dc grids and grid integration of distributed energy resources.

Dr. Kish was the recipient of the First Place Prize Paper Award in 2016 for the IEEE TRANSACTIONS ON POWER ELECTRONICS.

John Salmon (S'86–M'86) received the B.Sc. Eng. degree from Imperial College London, London, U.K., in 1982, the M.Eng. degree from McGill University, Montreal, QC, Canada, in 1984, and the Ph.D. degree from Imperial College London in 1987.

In 1987, he became an Assistant Professor with the Department of Electrical Engineering, University of Alberta, Edmonton, AB, Canada, where he has been a Full Professor since 1996. He was elected Chair of the same Department, in 2014. He has conducted research on utility connected converters for many years. His general research interests include power electronic converter designs for many applications including machine drive systems, electric vehicles, smart electrical grid interface, high speed machine drives, and battery voltage balancing networks. He has conducted research on the application of coupled inductor inverters for utility rectifiers, machine drive systems and battery charging systems. His research work has included designing specialty pulsewidth-modulation techniques for novel power converter designs.

Dr. Salmon was the recipient of several prize paper awards over the years for the IEEE Workshop on Control and Modeling for Power Electronics (COMPEL) in 2019, the IEEE Industry Applications Society: Industrial Drives Committee in 2008, and the Industrial Power Converter Committee in 2010 and in 1994.